A high-resolution analysis of the $\tilde{C}\,^2A_1-\tilde{X}\,^2A_1$ transition of $CaNH_2$: Pure precession in polyatomic molecules

Zulfikar Morbi, Chunfeng Zhao, and Peter F. Bernath
Center for Molecular Beams and Laser Chemistry, Department of Chemistry, University of Waterloo, Waterloo, Ontario, Canada, N2L 3G1

(Received 19 September 1996; accepted 17 December 1996)

The high resolution spectrum of the 0_0^0 vibronic band of the $\tilde{C}\,^2A_1-\tilde{X}\,^2A_1$ transition of $CaNH_2$ was recorded with a laser ablation/supersonic molecular beam spectrometer. Approximately 140 lines of the $K_a'=0\leftarrow K_a''=0$ and the $K_a'=1\leftarrow K_a''=1$ sub–bands were measured and combined with the previous $\tilde{A}\,^2B_2-\tilde{X}\,^2A_1$ and $\tilde{B}\,^2B_1-\tilde{X}\,^2A_1$ results. A global fit of the data was carried out and the effective spectroscopic constants for the $\tilde{X}$, $\tilde{A}$, $\tilde{B}$, $\tilde{C}$ states are reported. A complete set of spin–rotation constants ($\epsilon_{\alpha\alpha}$'s) are now available for the $\tilde{A}\,^2B_2$, $\tilde{B}\,^2B_1$ and $\tilde{C}\,^2A_1$ states. The unpaired electron in these three excited states can be considered to be located in three p–orbitals (p_x, p_y, p_z) centered on the metal atom. The simple pure precession model provides estimates for the 9 spin–rotation parameters in the $\tilde{A}$, $\tilde{B}$, and $\tilde{C}$ states. © *1997 American Institute of Physics.* [S0021-9606(97)00912-4]

I. INTRODUCTION

There has been a recent resurgence of interest in spectroscopic studies of the alkaline earth–containing polyatomic molecules. The molecules CaOH,[1,2] SrOH,[3] and CaCCH (Refs. 4–6) have been studied using a high temperature source called a Broida oven.[7] Much of the new work, however, has been carried out with the supersonic molecular beam technique which has allowed the study of large polyatomic molecules at high resolution. The low rotational (5–20 K) and vibrational ($\sim$300 K) temperatures allows detailed information such as the fine structure, hyperfine structure, asymmetry splittings and dipole moments to be extracted from the spectra. The most novel and interesting examples from this family of molecules are the alkaline earth half-sandwich molecules,[8] which were studied in great detail by the Miller group.[9–14] The high resolution experiments illustrate the wealth of spectroscopic information that can be obtained. Related studies include recent experiments on the singly charged alkaline earth–containing complexes such as $Ca^+(H_2O)$,[15] $Mg^+(H_2O)$ (Ref. 16) and their deuterated analogs. The electronic transitions of these molecules occur at higher energy ($\geqslant$21 500 cm^{-1}) compared to those of the isoelectronic $CaNH_2$ and $MgNH_2$ molecules.

The alkaline earth–containing polyatomic molecules were first studied by Harris and co-workers[1,3,17] and then further extended by Bernath and co-workers.[18–24] These researchers used a Broida–type oven, which is a relatively high temperature (400–500 K) molecular source that is convenient for Doppler–limited studies.[25] For a non–linear polyatomic molecule, the information available from these spectra is limited due to congestion by many overlapping lines. Thus, only a partial vibronic analysis was possible for most of the non–linear polyatomic molecules.[8,26–30]

The Broida oven work illustrated the close connection between the spectra of the polyatomic alkaline earth derivatives and the well understood spectra of the alkaline earth monohalide molecules. The basic properties of the monohalides (e.g. electronic origins, spin-orbit splittings, lifetimes, dipole moments, etc., . . .) are well described by the ligand field model proposed by Rice, Martin and Field.[31] This model treats the ligand (X^-) as a point charge that influences the non-bonding valence electron on the metal (M^+) ion. For example, the Ca^+ ion is perturbed by the electrostatic field of the fluoride anion (F^-), with the Ca^+ ion modelled as a closed shell Ca^{2+} core with a single valence electron. The approach of the F^- ligand destroys the spherical symmetry of the 4s atomic orbital and gives rise to the $X\,^2\Sigma^+$ state of the CaF molecule (Fig. 1).

Electronic excitation can be considered as transitions of this 4s electron to a predominately 4p orbital ''belonging'' to the Ca^+ ion. The doubly degenerate $4p\pi$ orbitals give rise to the $A\,^2\Pi$ state, while the $4p\sigma$ orbital results in the $B\,^2\Sigma^+$ excited state of the CaF molecule. Orbital mixing calculations were performed for CaF by Rice *et al.* showed that the X state has $\sim$80% $4s\sigma$ character and $\sim$20% $4p\sigma$, while the $A\,^2\Pi$ state was a 70:30 mixture of $4p\pi$ and $3d\pi$ and the $B\,^2\Sigma^+$ state is approximately a 50:50 mixture of $4p\sigma$ and $3d\sigma$.

Further extension of the ligand field model is made by substituting the fluoride ligand with various polyatomic ligands such as OH^-,[32] CCH^-, SH^-, NH_2^-, $C_5H_5^-$. This replacement lowers the symmetry of the molecule from $C_{\infty v}$ to C_{2v} for the NH_2^- ligand. In the $CaNH_2$ molecule, the $A\,^2\Pi$ state of CaF is further split into an in-plane ($\tilde{A}\,^2B_2$ state) and an out-of-plane ($\tilde{B}\,^2B_1$) state (Fig. 1). The energy ordering of the $\tilde{A}$ and $\tilde{B}$ states can be deduced using a simple argument. There is a lone pair of electrons in a nitrogen 2p_x orbital perpendicular to the plane of the NH_2^- ligand. If the lone electron ''belonging'' to Ca^+ occupies the $4p\pi_x$ ($\tilde{B}\,^2B_1$) orbital which is also perpendicular to the molecular plane, there will be greater electron–electron repulsion than if the lone electron occupied the $4p\pi_y$ orbital

 0021-9606/97/106(12)/4860/9/$10.00

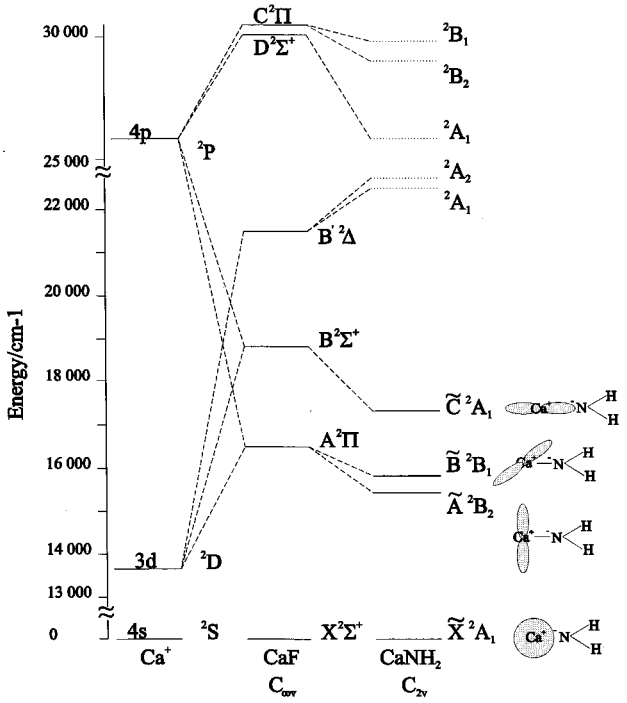

FIG. 1. The correlation of atomic Ca^+ orbitals with the electronic states of CaF and $CaNH_2$. The solid lines represent known energy levels and the dashed lines are predicted (Ref. 33) but not observed experimentally.

($\tilde{A}\ ^2B_2$) parallel to the plane of the molecule (see Fig. 2). Thus the $^2B_2$ state lies lower in energy than the $^2B_1$ state and this has been confirmed by *ab initio* electron propagator calculations by Ortiz.[33]

Törring *et al.*[34] proposed another model to describe the electronic structure of the alkaline earth monohalides. Their ionic model allows for a displacement of the unpaired valence electron in order to take into account the polarization of this electron away from the ligand. The paper by Mestadagh *et al.*[32] states that the Törring model is more flexible than the Rice model when dealing with polyatomic ligands such as OH^-. They extended the Törring *et al.* model to calculate dipole moments, bond dissociation energies and the location of excited electronic states for CaOH, SrOH and BaOH.[32] The calculation of the dipole moments are in very good agreement with the ground state experimental dipole moments [for CaOH and SrOH (Ref. 35)] which were not available to them at the time of publication. A natural extension of this work would be to carry out similar calculations for non-linear ligands such as NH_2^-.

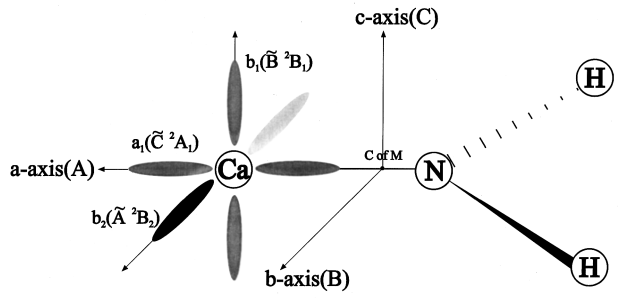

FIG. 2. The direction of the principal axes and the atomic orbitals of Ca^+ which give rise to the electronic states of $CaNH_2$. This diagram should be compared with the correlation diagram of Fig. 1.

The first spectroscopic investigation of $CaNH_2$ was completed by Wormsbecher *et al.*[36] in a Broida oven. A partial analysis of the 0_0^0 band of the $\tilde{C}\ ^2A_1$–$\tilde{X}\ ^2A_1$ transition was carried out but our measurements on cold $CaNH_2$ molecules are not completely consistent with their reported line positions. Whitham *et al.*[37] used the laser ablation/molecular beam technique to produce $CaNH_2$ but their studies were limited by the resolution of the probe laser (0.15 cm^{-1}) and consequently, only a partial analysis of the 0_0^0 bands of the $\tilde{A}\ ^2B_2$–$\tilde{X}\ ^2A_1$ and $\tilde{B}\ ^2B_1$–$\tilde{X}\ ^2A_1$ systems was performed. Marr *et al.*[38] recorded the first fully resolved high resolution spectrum of $CaNH_2$. They recorded the 0_0^0 band of the $\tilde{A}\ ^2B_2$–$\tilde{X}\ ^2A_1$ system, from which they derived rotational constants and measured the dipole moments of the $\tilde{A}$ and $\tilde{X}$ states. The 0_0^0 band of the $\tilde{B}\ ^2B_1$–$\tilde{X}\ ^2A_1$ system was analyzed by Zhao *et al.*,[39] we report here a high resolution analysis of the 0_0^0 bands of the $\tilde{C}\ ^2A_1$– $\tilde{X}\ ^2A_1$ band system. $CaNH_2$ is the first non–linear alkaline earth derivative where all four of the ($\tilde{X}$, $\tilde{A}$, $\tilde{B}$, $\tilde{C}$) low–lying electronic states are characterized at high resolution, thus we shall discuss the application of the simple ''pure precession'' model to polyatomic systems of low symmetry.

II. EXPERIMENT

$CaNH_2$ was produced using a pulsed laser ablation supersonic molecular beam spectrometer. Details of the experimental setup were provided in a previous paper (Zhao *et al.*[40]) with the exception that a skimmer was not used in the experiments described here. Briefly, a rotating calcium rod was vaporized with the second harmonic of a pulsed Nd:YAG laser and approximately 5% NH_3 seeded in Ar(or He) was allowed to react with the metal vapor. A backing pressure of 50 psi was maintained behind the pulsed valve (General Valve). The probe laser, an argon ion pumped Coherent 699-29 cw ring dye laser (R6G dye), was crossed with the molecular beam ~15 cm downstream from the nozzle. The laser–induced fluorescence signal was viewed through a 600 nm ± 5 nm bandpass filter and focused onto a cooled GaAs photomultiplier tube.

A boxcar averager was used to gate the signal and for the experiment using Ar seed gas, the boxcar delay was 200 μs after the YAG pulse, while a 85 μs delay was used for the He experiment. In both experiments the boxcar gate was open for ~20 μs. The LIF signal was monitored in 50 MHz steps of the probe laser which was scanned at a rate of 60 seconds per 10 GHz. Typical linewidth (full width at half maximum) was of the order of 150–200 MHz. Calibration of the laser was achieved by simultaneously recording the laser excitation spectrum of I_2,[41,42] giving an absolute accuracy of ± 0.0035 cm^{-1} for the measured line positions.

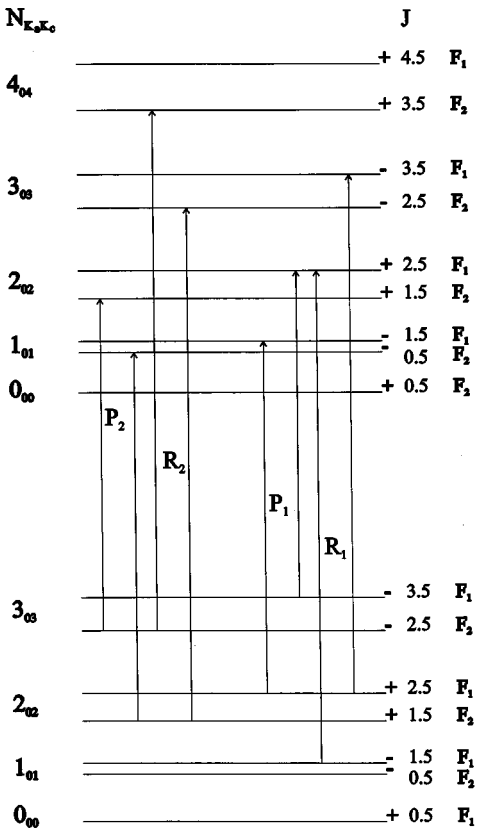

FIG. 3. The energy level diagram associated with the $K_a''=0\leftarrow K_a'=0$ sub–band of the $\tilde{C}\ ^2A_1$–$\tilde{X}\ ^2A_1$ transition of $CaNH_2$. The allowed transition are labeled by $\Delta J_{F_i''}(i=1,2)$.

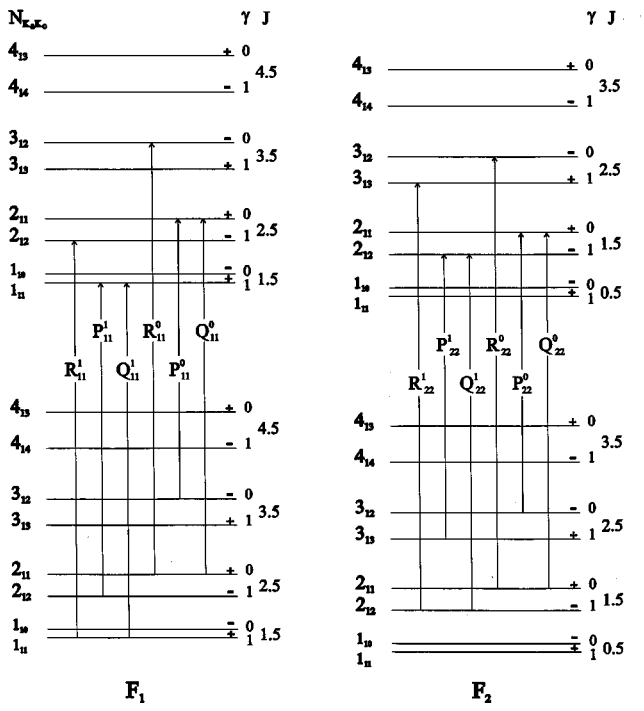

FIG. 4. The allowed transition of the $K_a''=1\leftarrow K_a'=1$ sub–band of the $\tilde{C}\ ^2A_1$–$\tilde{X}\ ^2A_1$ transition. Each transition is labeled by $\Delta J^{\gamma}_{F_i'',F_i'}(i=1,2)$, see text for details.

III. OBSERVATIONS

The approximate positions of the $\tilde{A}\ ^2B_2$— $\tilde{X}\ ^2A_1$, $\tilde{B}\ ^2B_1$— $\tilde{X}\ ^2A_1$ and $\tilde{C}\ ^2A_1$— $\tilde{X}\ ^2A_1$ band origins were known from the low resolution work of Bopegedera *et al.*[43] and also from Wormsbecher *et al.*[36] Thus, the laser was scanned at high resolution from 17 365 cm^{-1} to 17 395 cm^{-1} to measure the spectrum of the $\tilde{C}\ ^2A_1$— $\tilde{X}\ ^2A_1$ system. Rotational structure of the spectrum was consistent with the parallel band structure of an a–type transition. The selection rules for a doublet a–type transition are $\Delta K_a=0$, $\Delta K_c=\pm 1$, $\Delta J=\pm 1$, $F_1\rightarrow F_1$, $F_2\rightarrow F_2$ for a $K_a'=0\leftarrow K_a''=0$ sub–band, while for a $K_a'=1\leftarrow K_a''=1$ sub–band a Q–branch ($\Delta J=0$) is also allowed. It is useful to introduce the label, γ, for the rotational energy levels (Jarman *et al.*[22]), where $\gamma=K_a+K_c-N$, and γ can take values of 0 or 1. Therefore, we can have $\gamma'=0\leftarrow\gamma''=0$ for a $K_a=0$—0 sub–band and both $\gamma'=0\leftarrow\gamma''=0$ and $\gamma'=1\leftarrow\gamma''=1$ for a $K_a=1$—1 sub–band.

The allowed transitions of the $K_a=0$—0 sub-band are depicted in Fig. 3. Each rotational level labeled $N_{Ka,Kc}$ is split into two fine structure levels by spin–rotation interactions, and are labeled F_1 for $J=N+\frac{1}{2}$ and F_2 for $J=N-\frac{1}{2}$. Only P and R branches for the $K_a=0$—0 sub-band are allowed so the rotational spectrum is analagous to a $^2\Sigma$—$^2\Sigma$ transition of a diatomic molecule. Figure 4 shows the corresponding energy level diagram for a $K_a=1$—1 sub-band. In this case each rotational level is split into four components because of spin–rotation interactions (F_1 and F_2) and also due to asymmetry doubling ($\gamma=0$ or 1, indicated by a superscript). Thus, the $K_a=1$—1 sub-band resembles a Hund's case (b)$^2\Pi$—Hund's case (b)$^2\Pi$ transition of a diatomic molecule.

Figure 5 shows the overview of the $\tilde{C}$–$\tilde{X}$ band system recorded in Ar and in He. The He spectrum has a slightly higher rotational temperature (T_{rot} = 13 K) than the Ar spectrum (T_{rot} = 6 K). Initially the Ar spectrum was used for data analysis, but the F_2 component of the $K_a=1$—1 sub–band was absent. Subsequently the higher temperature He spectrum was used for the analysis and we were able to obtain J values as high as $19\frac{1}{2}$ for the $K_a=0$—0 sub-band and J $=14\frac{1}{2}$ for the $K_a=1$—1 sub-band. Some of the assigned transitions of the spectrum are shown in Figure 6. All of the allowed branches (4 for $K_a=0$—0, 12 for $K_a=1$—1) were seen in this spectrum, however, it was found that the transitions involving the F_2 component of the $K_a=1$—1 sub-band were very weak.

IV. RESULTS

The $\tilde{C}$–$\tilde{X}$ band system is an a–type transition so that the transition dipole moment is along the Ca–N bond. The $\Delta K_a = 0$ selection rule means that all of the sub–bands with different K_a will have approximately the same origin, leading to a very congested spectrum. Fortunately, with the rotational cooling in a molecular beam only two K_a'' values had

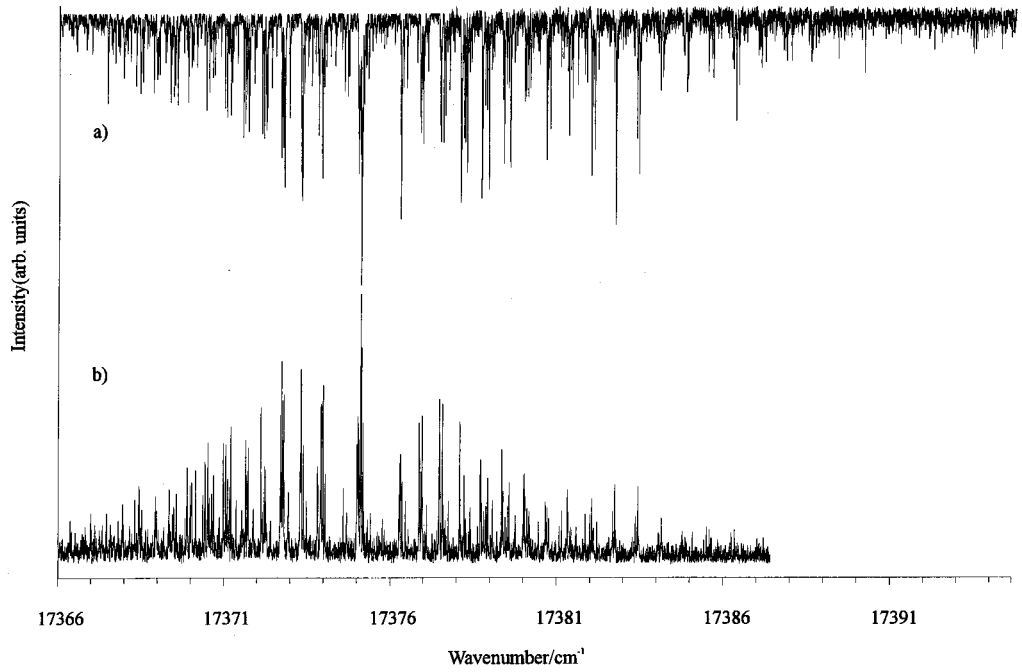

FIG. 5. An overview of the high resolution spectrum of the 0_0^0 vibronic band of the $\widetilde{C}\ ^2A_1$–$\widetilde{X}\ ^2A_1$ transition (a) recorded in He (b) Ar.

significant population ($K_a = 0,1$). Because of nuclear spin statistics, the $K_a = 1$ rotational levels (ortho) cannot cool into the $K_a = 0$ (para) levels. Preliminary experiments, (performed at Waterloo) using a Broida oven showed that the spectrum of the $\widetilde{C}$–$\widetilde{X}$ system was extremely dense, with many K_a–rotational sub–bands and vibrational hot bands present. The spectra recorded in this way were found to be extremely difficult to analyze.

The analysis of the $\widetilde{C}$–$\widetilde{X}$ spectrum was partially aided by a Loomis–Wood program to sort out the branches. Although

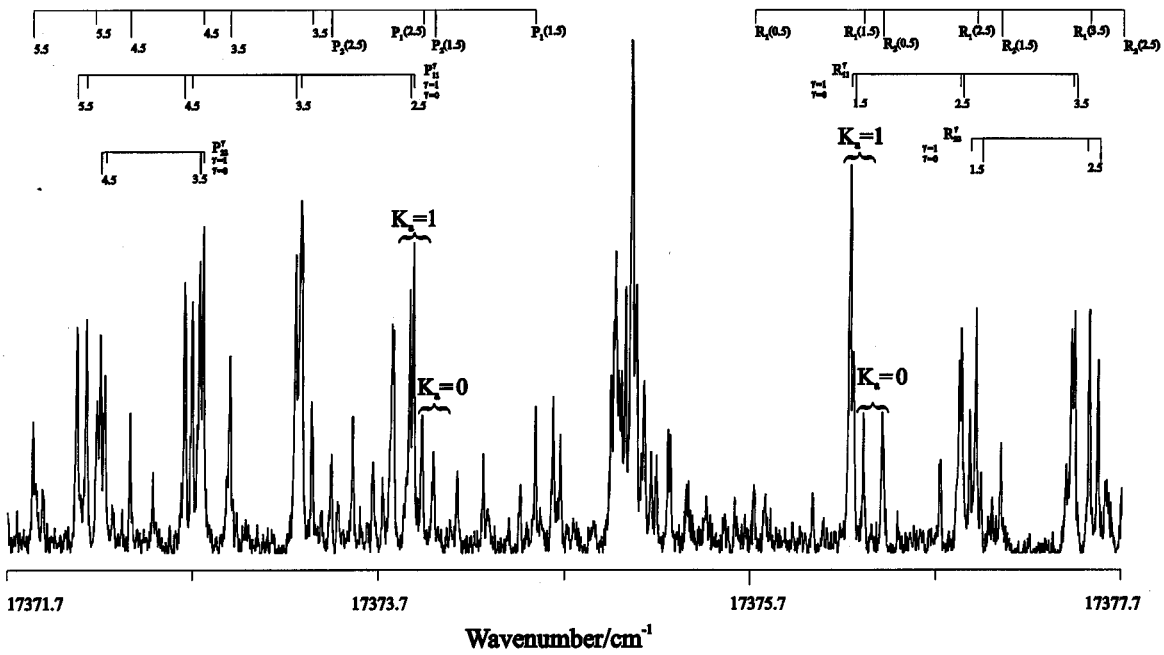

FIG. 6. A portion of the high resolution spectrum of the 0_0^0 band of the $\widetilde{C}\ ^2A_1$–$\widetilde{X}\ ^2A_1$ transition of $CaNH_2$ near the origin. This spectrum was recorded with He gas. Note the 2:1 intensity ratio of ortho ($K_a=1$) and para ($K_a=0$) levels and the small asymmetry splitting (γ) of the $K_a''=1 \leftarrow K_a'=1$ sub–band. The Q–branch transitions are not labeled for clarity.

TABLE I. Spectroscopic constants for $CaNH_2$ (cm^{-1}).

	$\widetilde{X}\ ^2A_1$	$\widetilde{A}\ ^2B_2$	$\widetilde{B}\ ^2B_1$	$\widetilde{C}\ ^2A_1$
T_{0-0}	0	15464.36739(48)	15885.28188(99)	17375.16688(67)
A	13.05744(55)	11.44854(14)	14.3664(14)	12.9512(89)
$\frac{1}{2}(B+C)$	0.296652(11)	0.303107(15)	0.301693(21)	0.301512(15)
$\frac{1}{4}(B-C)$	$1.8894(44)\times10^{-3}$	$1.958(28)\times10^{-3}$	$4.68(79)\times10^{-3}$	$1.771(10)\times10^{-3}$
ϵ_{aa}	0	8.2369(12)	−7.5472(19)	0.9986(61)
$\frac{1}{2}(\epsilon_{bb}+\epsilon_{cc})$	$8.515(672)\times10^{-4}$	$3.0534(17)\times10^{-2}$	$2.083(13)\times10^{-2}$	$-3.9134(10)\times10^{-2}$
$\frac{1}{4}(\epsilon_{bb}-\epsilon_{cc})$	0	$-1.2617(14)\times10^{-2}$	$-8.66(17)\times10^{-3}$	$-3.28(175)\times10^{-4}$
D_K	–	–	$-4.040(29)\times10^{-2}$	–
D_N	–	–	$-1.09(13)\times10^{-6}$	$1.088(25)\times10^{-6}$
δ_K	–	–	$2.160(74)\times10^{-3}$	–
Δ_K^S	–	$-6.065(30)\times10^{-2}$	$-1.46(17)\times10^{-2}$	–
Δ_{KN}^S	–	–	$-6.67(16)\times10^{-2}$	–
Δ_{NK}^S	–	–	$5.90(17)\times10^{-3}$	$2.54(20)\times10^{-3}$

this procedure[44] is extremely useful in the analysis of congested spectra of $^1\Sigma$ diatomic molecules, more care must be taken with non–linear molecules and non–$^1\Sigma$ diatomics. This is because the line spacing of P and R branches that are connected can be quite different. For $CaNH_2$, a particular P or R branch can be found rather easily, but connecting the P and R branches was difficult. With the help of the spectroscopic constants of Marr *et al.*,[38] ground state combination differences were used to connect the branches. Once a single branch of the $K_a'=0\leftarrow K_a''=0$ sub-band was assigned and fitted with a non–linear least squares program, the remaining branches were then assigned by prediction. The same procedure was used to assign the lines of the $K_a'=1\leftarrow K_a''=1$ sub-band.

The data were fit using the effective rotational Hamiltonian (A–reduction) of Watson[45] and the spin–rotation Hamiltonian of Brown *et al.*[46] The spin–rotation Hamiltonian is written as:

$$\hat{H}_{\rm sr}=\frac{1}{2}\sum_{\alpha,\beta}\epsilon_{\alpha\beta}(\hat{\rm N}_\alpha\hat{\rm S}_\beta+\hat{\rm S}_\beta\hat{\rm N}_\alpha), \tag{1}$$

where α and β are the principal rotation axes. A total of nine spin rotation constants are possible, but for a molecule with orthorhombic (C_{2v}) symmetry only three, ϵ_{aa}, ϵ_{bb} and ϵ_{cc}, are non-zero. It will be shown (see below) that these constants are determined by second order spin–orbit interactions rather than true spin–rotation interactions. The matrix elements used in the non–linear least squares program were taken from the literature (Watson,[47] Hirota[48]). For the final fit the $\widetilde{A}\ ^2B_2$–$\widetilde{X}\ ^2A_1$ lines of Marr *et al.*,[38] the $\widetilde{B}\ ^2B_1$– $\widetilde{X}\ ^2A_1$ lines of Zhao *et al.*[39] were added to this data set[49] and a global fit of all the data was done. The rotational constants for the $\widetilde{X}\ ^2A_1$, $\widetilde{A}\ ^2B_2$, $\widetilde{B}\ ^2B_1$, $\widetilde{C}\ ^2A_1$ states are reported in Table I.

V. DISCUSSION

A. Pure precession model

The most interesting of the spectroscopic constants listed in Table I are the spin–rotation constants ($\epsilon_{\alpha\alpha}$). This is because we can use the simple pure precession model to give a physical picture of the orbitals containing the unpaired electron. $CaNH_2$ is the first of the alkaline earth polyatomic molecules for which all of the low–lying electronic states are known so a discussion of the pure precession is warranted. In this model we will assume that only pure p–type orbitals give rise to the first three excited electronic states (Fig. 2) of $CaNH_2$ while the ground state has the unpaired electron in an s–type orbital.

The theory of spin–rotation interactions was first considered by Van Vleck.[50] There are two major contributions to these parameters, a direct magnetic coupling between the electronic spin and molecular rotation, and a second order spin–orbit coupling between the electron spin and the unquenched angular momentum of the unpaired electron.[51] It has been shown (Curl,[52] Dixon[53]) that the major contribution to the spin–rotation constants is the second order spin–orbit interaction.

The Hamiltonian for rigid rotation of a polyatomic molecule in the molecular frame with the inclusion of spin–orbit interaction is written as:

$$\hat{\rm H}=A(\hat{\rm N}_{\rm a}-\hat{\rm L}_{\rm a})^2+B(\hat{\rm N}_{\rm b}-\hat{\rm L}_{\rm b})^2+C(\hat{\rm N}_{\rm c}-\hat{\rm L}_{\rm c})^2 + \sum_j \hat{\boldsymbol{\eta}}_{\mathbf{j}}\cdot\hat{\mathbf{s}}_{\mathbf{j}}. \tag{2}$$

Here $\hat{\rm N}$ is the total angular momentum excluding spin, $\hat{\rm L}$ is the electronic angular momentum, (a,b,c) are the principal axes in the molecular frame and the sum j is over all electrons in the system. From equation (2) we can see that the purely rotational part of the Hamiltonian is:

$$\hat{\rm H}_{\rm rot}=A\hat{\rm N}_{\rm a}^2+B\hat{\rm N}_{\rm b}^2+C\hat{\rm N}_{\rm c}^2, \tag{3}$$

and the perturbation of strict rigid rotation arises from the cross terms between:

$$\hat{\rm H}_1=-2A\hat{\rm N}_{\rm a}\hat{\rm L}_{\rm a}-2B\hat{\rm N}_{\rm b}\hat{\rm L}_{\rm b}-2C\hat{\rm N}_{\rm c}\hat{\rm L}_{\rm c} \text{ and}$$

$$\hat{\rm H}_2=\sum_j \hat{\boldsymbol{\eta}}_{\mathbf{j}}\cdot\hat{\mathbf{s}}_{\mathbf{j}}. \tag{4}$$

Performing a Van Vleck transformation leads to the effective spin-rotation Hamiltonian for a molecule with C_{2v} symmetry:

$$\hat{H}_{sr}=\epsilon_{aa}\hat{N}_a\hat{S}_a+\epsilon_{bb}\hat{N}_b\hat{S}_b+\epsilon_{cc}\hat{N}_c\hat{S}_c, \tag{5}$$

neglecting the quartic spin-rotation terms (for example see Duxbury[51] or Brown *et al.*[46]). It was shown by Dixon[53] that the second order spin–orbit corrections to the spin–rotation constants of a doublet state are:

$$\epsilon^{(2)}_{\alpha\alpha}=\sum_{n\neq 0}\sum_j \frac{4B_\alpha k_j\langle\psi_0|\hat{L}_\alpha|\psi_n\rangle\langle\psi_n|\hat{\eta}_{\alpha,j}|\psi_0\rangle}{E^o_n-E^o_0}. \tag{6}$$

The sum j is over all electrons, $k_j=+1$ for promotion of an unpaired electron, $k_j=-1$ for promotion of an electron into a half–filled orbital or zero otherwise. The B_α's in (6) are the rotational constants in the principle axis system (e.g. $B_a=A$, $B_b=B$, $B_c=C$). The matrix element involving $\hat{\eta}_{\alpha,j}$ can be written in terms of the one–electron orbital angular momentum operators, $\hat{\eta}_{\alpha,j}=\zeta_j\hat{\ell}_{\alpha,j}$, where ζ_j is the spin–orbit constant for the electron. In the pure precession limit, we can neglect all electrons except the unpaired valence electron on Ca^+. Thus we can remove the sum over j with a single term involving $\zeta_{3p}\hat{\ell}_\alpha$ leaving the second order correction to the spin–rotation constants as:

$$\epsilon^{(2)}_{\alpha\alpha}=\sum_{n\neq 0}\frac{4B_\alpha\langle\psi_0|\hat{\ell}_\alpha|\psi_n\rangle\langle\psi_n|\zeta_{3p}\hat{\ell}_\alpha|\psi_0\rangle}{E^o_n-E^o_0}. \tag{7}$$

A similar analysis as above can be done for the second order correction to the rotational constants (A,B,C). The result is:

$$B^{(2)}_\alpha=\sum_{n\neq 0}\frac{4B^2_\alpha\langle\psi_0|\hat{\ell}_\alpha|\psi_n\rangle^2}{E^o_0-E^o_n}. \tag{8}$$

It will be shown later that the second order correction to the A rotational constant is significant while the corrections to B and C are negligible.

A second simplification that can be made is the unique perturber approximation, where we assume that each electronic state interacts solely with a dominant perturbing state (Dixon[54]). In $CaNH_2$, rotation of the molecule about the a–axis causes interactions between the $\tilde{B}\ ^2B_1$ (p_x) and $\tilde{A}\ ^2B_2$ (p_y) states, rotation about the c–axis causes interactions between the $\tilde{C}\ ^2A_1$ (p_z) and the $\tilde{B}\ ^2B_1$ states and finally, rotation about the b–axis leads to interactions of the $\tilde{C}\ ^2A_1$ and $\tilde{A}\ ^2B_2$ states.

To obtain the second order correction of ϵ_{aa} in the $\tilde{A}\ ^2B_2$ state, one needs wavefunctions for the two interacting states ($\tilde{B}\ ^2B_1$, $\tilde{A}\ ^2B_2$) and the integrals $\langle\tilde{B}\ ^2B_1|\hat{\ell}_\alpha|\tilde{A}\ ^2B_2\rangle$, $\langle\tilde{A}\ ^2B_2|\zeta_{3p}\hat{\ell}_\alpha|\tilde{B}\ ^2B_1\rangle$ need to be evaluated. However, in the pure precession limit we assume that the electronic states arise strictly from pure p–type orbitals. In Table II, the correlation of the electronic states and the principal axis system with the (x,y,z) coordinate system is provided. Table III shows the effect of the one-electron orbital angular momentum operators on the three p–orbitals. Using these results

TABLE II. Correlation between principal axis system and molecular coordinates. See Fig. 2.

$\tilde{A}\ ^2B_2=p_y$	$\hat{\ell}_a=\hat{\ell}_z$
$\tilde{B}\ ^2B_1=p_x$	$\hat{\ell}_b=\hat{\ell}_y$
$\tilde{C}\ ^2A_1=p_z$	$\hat{\ell}_c=\hat{l}_x$

and equation (7) we can write the formula for the second order correction to ϵ_{aa} of the $\tilde{A}\ ^2B_2$ state as:

$$\epsilon^{(2)}_{aa}=\frac{4A\langle p_y|\hat{\ell}_z|p_x\rangle\langle p_x|\zeta_{3p}\hat{\ell}_z|p_y\rangle}{E_{\tilde{B}}-E_{\tilde{A}}}$$

$$=\frac{-4A\zeta_{3p}i^2}{E_{\tilde{B}}-E_{\tilde{A}}}=\frac{+4AA^{so}}{E_{\tilde{B}}-E_{\tilde{A}}}. \tag{9}$$

In the last step we replace ζ_{3p} with A^{so}, which is the spin–orbit splitting in the hypothetical linear molecule. Clearly one can see that we get the negative of equation (9) for ϵ_{aa} of the $\tilde{B}\ ^2B_1$ state . Performing similar calculations we get $\epsilon^{(2)}_{bb}=0$ for the $\tilde{A}\ ^2B_2$ state, $\epsilon^{(2)}_{cc}=0$ for the $\tilde{C}\ ^2A_1$ state and:

$$\epsilon^{(2)}_{bb}=\pm\frac{4BA^{so}}{E_{\tilde{C}}-E_{\tilde{B}}},\quad \epsilon^{(2)}_{cc}=\pm\frac{4CA^{so}}{E_{\tilde{C}}-E_{\tilde{A}}}. \tag{10}$$

In the above formulae the top sign corresponds to the lower electronic state of the interacting pair of states. The second order correction to the A rotational constant then becomes:

$$A^{(2)}=\pm\frac{4A^2}{E_{\tilde{B}}-E_{\tilde{A}}}. \tag{11}$$

One can see the close connection between the above results and the perturbation treatment of Whitham and Jungen.[37] They considered the rotation about the a-axis as equivalent to an a-axis Coriolis interaction with an off–diagonal spin–orbit coupling. The Hamiltonian for this interaction is:

$$\hat{H}_{int}=A^{so}\hat{L}_a\hat{S}_a-2A\hat{N}_a\hat{L}_a. \tag{12}$$

The a–axis of a (near) prolate symmetric top molecule plays the same role in quanitization as the internuclear axis of a diatomic molecule so they replaced the angular momentum operators $\hat{N}_a$, $\hat{L}_a$, $\hat{S}_a$ by their corresponding quantum numbers K_a, Λ and Σ. They then diagonalized the 2×2 energy matrix for the interacting $\tilde{A}$ and $\tilde{B}$ states, and solved for the correction to their energies to second order. The relevant results from their analysis are:

TABLE III. Effect of orbital angular momentum operators on the Cartesian p–orbitals.

$\hat{\ell}_x p_x=0$	$\hat{\ell}_y p_x=-ip_z$	$\hat{\ell}_z p_x=ip_y$
$\hat{\ell}_x p_y=ip_z$	$\hat{\ell}_y p_y=0$	$\hat{\ell}_z p_y=-ip_x$
$\hat{\ell}_x p_z=-ip_y$	$\hat{\ell}_y p_z=ip_x$	$\hat{\ell}_z p_z=0$

TABLE IV. Spin rotation parameters.

		$\widetilde{X}\ ^2A_1$	$\widetilde{A}\ ^2B_2$	$\widetilde{B}\ ^2B_1$	$\widetilde{C}\ ^2A_1$
	Observed	0	8.236	−7.547	0.998
ϵ_{aa}	Pure Precession	0	8.193	−8.193	0
	Formula [a]	–	$+\frac{4\Lambda^2 AA^{so}}{\Delta E_{\widetilde{B}-\widetilde{A}}}$	$-\frac{4\Lambda^2 AA^{so}}{\Delta E_{\widetilde{B}-\widetilde{A}}}$	–
	Observed	8.5×10^{-4}	0.00530	0.00351	−0.0398
ϵ_{bb}	Pure Precession	0	0	0.0539	−0.0547
	Formula	–	–	$+\frac{2\ell(\ell+1)BA^{so}}{\Delta E_{\widetilde{C}-\widetilde{B}}}$	$-\frac{2\ell(\ell+1)BA^{so}}{\Delta E_{\widetilde{C}-\widetilde{B}}}$
	Observed	8.5×10^{-4}	0.0558	0.0381	−0.0385
ϵ_{cc}	Pure Precession	0	0.0418	0	−0.0417
	Formula	–	$+\frac{2\ell(\ell+1)CA^{so}}{\Delta E_{\widetilde{C}-\widetilde{A}}}$	–	$-\frac{2\ell(\ell+1)CA^{so}}{\Delta E_{\widetilde{C}-\widetilde{A}}}$

[a] $A^{so} = 66.795\ cm^{-1}$ spin–orbit constant of CaOH.

$$A = A^{spec} \pm \frac{4\Lambda^2 A^2}{E_{\widetilde{B}} - E_{\widetilde{A}}}, \quad \epsilon_{aa}^{(2)} = \pm \frac{4\Lambda^2 AA^{so}}{E_{\widetilde{B}} - E_{\widetilde{A}}}. \tag{13}$$

The formula for $\epsilon_{aa}^{(2)}$ is equivalent to the formula derived from the pure precession limit where we had already used the fact that $\Lambda = 1$ ($\Lambda \equiv$ the projection of the electronic orbital angular momentum on the top axis) for a p–orbital. A^{spec} is the rotational constant derived from fitting the line positions of the spectra, and again the top sign of equation (13) refers to the lower electronic state. This result also shows that the observed value of the A^{spec} rotational constant contains a large second order contribution to the true A rotational constant.

On the basis of the molecular geometry, $\Delta A = A_{\widetilde{B}}^{spec} - A_{\widetilde{A}}^{spec}$ should be small since the electron occupies an in–plane or an out–of–plane ''non-bonding'' p–orbital. However, there is a significant difference between the A's ($A_{\widetilde{A}}^{spec} = 11.449\ cm^{-1}$ and $A_{\widetilde{B}}^{spec} = 14.366\ cm^{-1}$) which would at first sight imply a large change in geometry. Applying the second order correction from equation (13) we find that the true rotational constant for the $\widetilde{A}$ and $\widetilde{B}$ states is $12.907\ cm^{-1}$, which is very close to the $A^{spec} = 12.951\ cm^{-1}$ for the $\widetilde{C}$ state and to the $A^{spec} = 13.057\ cm^{-1}$ of the ground state. The second order corrections to the B (where $B^{(2)} = \pm(4B^2/E_{\widetilde{C}} - E_{\widetilde{B}})$) and C rotational constants are small ($\sim 10^{-4}\ cm^{-1}$) compared to experimental uncertainty of these constants.

The approach given by Whitham and Jungen is specific to the $\widetilde{A}$ and $\widetilde{B}$ states and interactions about the a–axis. Our discussion here is more general and for an electron that possesses a well defined orbital angular momentum we can write effective formulae for ϵ_{bb} and ϵ_{cc}:

$$\epsilon_{bb}^{(2)} = \pm \frac{2\ell(\ell+1)BA^{so}}{E_{\widetilde{C}} - E_{\widetilde{B}}}, \quad \epsilon_{cc}^{(2)} = \pm \frac{2\ell(\ell+1)CA^{so}}{E_{\widetilde{C}} - E_{\widetilde{A}}}, \tag{14}$$

where $\ell = 1$ for p orbitals.

The comparison of the observed spin–rotation contents to their corresponding pure precession values are shown in Table IV. The values calculated from the pure precession formula are in reasonable agreement with the observed spin rotation parameters in both magnitude and sign. The ϵ_{aa} parameter is well predicted in the $\widetilde{A}$, $\widetilde{B}$ states, i.e. within 10 % of the experimental value. Also, the spin–rotation parameters in the ground state are predicted to be zero by pure precession and experimentally we find an extremely small value for $\frac{1}{2}(\epsilon_{bb} + \epsilon_{cc})$. For a ground state that correlates to a $^2\Sigma^+$ state in a linear configuration, the expected spin rotation parameter, γ, would be small. Since $\frac{1}{2}(\epsilon_{bb} + \epsilon_{cc})$ is equivalent to the γ constant of a linear molecule, the size of $\frac{1}{2}(\epsilon_{bb} + \epsilon_{cc}) = 8.5\times10^{-4}\ cm^{-1}$ should be close to that of CaOH ($\gamma' = 9.53\times10^{-4}\ cm^{-1}$) or CaF ($\gamma' = 1.3\times10^{-3}\ cm^{-1}$). The parameter ϵ_{aa} is equivalent to the spin–orbit (A) constant of a linear molecule, which is zero for a $^2\Sigma^+$ state. The other spin–rotation parameters of Table IV are in good qualitive agreement with the pure precession values except for ϵ_{aa} of the $\widetilde{C}\ ^2A_1$ state and ϵ_{bb} of the $\widetilde{B}\ ^2B_1$ state. This is most likely due to mixing of the pure p–orbitals (assumed in our pure precession model) with d–orbitals. This is further supported by the higher order quartic spin-rotation parameters ($\Delta_{NK}^S, \Delta_{KN}^S, \Delta_K^S$) that are required to adequately fit the transitions to the $\widetilde{B}\ ^2B_1$ state.

Finally, we have calculated values for the g–tensor from Curl's formula:[55]

$$g_{\alpha\alpha} = g_e - \frac{\epsilon_{\alpha\alpha}}{2B_\alpha}, \tag{15}$$

where g_e is the electron g–factor. The predicted values are reported in Table V.

TABLE V. Estimated g–tensor from Curl's formula.

	$\widetilde{X}\ ^2A_1$	$\widetilde{A}\ ^2B_2$	$\widetilde{B}\ ^2B_1$	$\widetilde{C}\ ^2A_1$
g_{aa}	2.0023	1.6426	2.2650	1.9638
g_{bb}	2.0009	1.9937	1.9965	2.0675
g_{cc}	2.0009	1.9091	1.9369	2.0669

TABLE VI. Geometrical parameters.

	$\widetilde{X}\ ^2A_1$	$\widetilde{A}\ ^2B_2$		$\widetilde{B}\ ^2B_1$	$\widetilde{C}\ ^2A_1$
θ_{HNH}	100.5°	101.3°		101.3°	101.1°
r_{NH} (Å) [a]			1.041		
r_{CaN} (Å)	2.118	2.098		2.123	2.102
θ_{HNH}	102.9°	103.8°		103.8°	103.5°
r_{NH} (Å)[b]			1.025		
r_{CaN} (Å)	2.140	2.120		2.145	2.125

[a]Bond distance from NH_2^-, Ref. 56.
[b]Bond distance from NH_2, Ref. 57.

B. Geometrical parameters

We have calculated r_0 geometries for all of the low–lying states of $CaNH_2$. Rotational constants are available for only one isotopomer ($^{40}Ca^{14}NH_2$), so that all three structural parameters r_{CaN}, r_{NH}, and θ_{HNH} cannot be determined simultaneously for the planar $CaNH_2$ molecule. The inertial defects are 0.16, 0.13, 0.45 and 0.01 amu Å^2 for the $\widetilde{X}$, $\widetilde{A}$, $\widetilde{B}$ and $\widetilde{C}$ states, respectively. Thus, the r_{NH} bond distance was constrained to the value found in NH_2^- (Ref. 56) $r_{NH}=1.041$ Å or NH_2 (Ref. 57) $r_{NH}=1.023$ Å. For the $\widetilde{A}$ and $\widetilde{B}$ states we used the true value of the A rotational constant to calculate I_A. Fundamental constants and molecular masses were taken from Ref. 58. In each case we calculated the geometry with (I_A,I_B) or (I_A,I_C) pairs. Table VI and VII show the results of the calculation, which are the average of the moment of inertia pairs, and these are compared with r_e *ab initio* calculations[59] performed for $CaNH_2$. The theoretical values are in reasonable agreement with experiment, except for the HNH angle.

VI. CONCLUSIONS

The high resolution spectrum of the $\widetilde{C}\ ^2A_1$–$\widetilde{X}\ ^2A_1$ band system of $CaNH_2$ has been recorded and analyzed. $CaNH_2$ is the first alkaline–earth polyatomic molecule for which high resolution data are available for the first three excited states. We used the pure precession model to predict the spin–rotation parameters for this molecule. This model confirms the simple one–electron hydrogenic picture often used for diatomic alkaline–earth molecules is also useful for non–linear polyatomic molecules such as $CaNH_2$.

TABLE VII. Experimental and *ab initio* parameters for the $\widetilde{X}\ ^2A_1$ state.

		DFT [a]	Expt.	
θ_{HNH}		127.2°	100.5°	102.9°
r_{NH} (Å)		1.02	1.041[b]	1.025[b]
r_{CaN} (Å)		2.13	2.118	2.140
Vibration		DFT (cm^{-1})[a]	Expt. ($\pm$ 10 cm^{-1})[c]	
ν_6 anti–symm. NH bend	b_2	345	320	
ν_4 out–of–plane bend	b_1	455	347	
ν_3 Ca–N stretch	a_1	544	520	
ν_2 symm. NH bend	a_1	1586	–	
ν_1 symm. NH stretch	a_1	3448	–	
ν_5 anti–symm. NH stretch	b_2	3535	–	

[a]Reference 59.
[b]Fixed, see text.
[c]From low resolution Broida oven experiment.

ACKNOWLEDGMENTS

This work is supported by Natural Sciences and Engineering Research Council of Canada (NSERC). Z. M. also wishes to thank NSERC for a graduate scholarship. We thank W. Chan and I. Hamilton for providing us with the results of their calculations in advance of publication.

[1] R.C. Hilborn, Z. Qingshi, and D.O. Harris, J. Mol. Spectrosc. **97**, 73 (1983).
[2] P.F. Bernath and C.R. Brazier, Astrophys. J. **288**, 373 (1985).
[3] J. Nakagawa, R.F. Wormsbecher, and D.O. Harris, J. Mol. Spectrosc. **97**, 37 (1983).
[4] A.M.R.P. Bopegedera, C.R. Brazier, and P.F. Bernath, Chem. Phys. Lett. **136**, 97 (1987).
[5] A.M.R.P. Bopegedera, C.R. Brazier, and P.F. Bernath, J. Mol. Spectrosc. **129**, 268 (1988).
[6] M. Li and J.A. Coxon, J. Mol. Spectrosc. **176**, 206 (1996).
[7] J.B. West, R.S. Bradford, J.D. Eversole, and C.R. Jones, Rev. Sci. Instrum. **46**, 164 (1975).
[8] L.C. O'Brien and P.F. Bernath, J. Am. Chem. Soc. **108**, 5017 (1986).
[9] T.M. Cerny, J.M. Williamson, and T.A. Miller, J. Chem. Phys. **102**, 2372 (1995).
[10] A.M. Ellis, E.S.J. Robles, and T.A. Miller, J. Chem. Phys. **94**, 1752 (1991).
[11] E.S.J. Robles, A.M. Ellis, and T.A. Miller, J. Am. Chem. Soc. **114**, 7171 (1992).
[12] E.S.J. Robles, A.M. Ellis, and T.A. Miller, J. Phys. Chem. **96**, 8791 (1992).
[13] E.S.J. Robles, A.M. Ellis, and T.A. Miller, J. Phys. Chem. **96**, 3247 (1992).
[14] E.S.J. Robles, A.M. Ellis, and T.A. Miller, J. Phys. Chem. **96**, 3258 (1992).
[15] C.T. Scurlock, S.H. Pullins, J.E. Reddic, and M.A. Duncan, J. Chem. Phys. **104**, 4591 (1996).
[16] K.F. Willey, C.S. Yeh, D.L. Robbins, J.S. Pilgrim, and M.A. Duncan, J. Chem. Phys. **97**, 8886 (1992).
[17] R.F Wormsbecher, M. Trkula, C. Martner, R.E. Penn, and D.O. Harris, J. Mol. Spectrosc. **97**, 29 (1983).
[18] C.R. Brazier and P.F. Bernath, J. Phys. Chem. **86**, 5918 (1987).
[19] L.C. O'Brien and P.F. Bernath, J. Chem. Phys. **88**, 2117 (1988).
[20] L.C. O'Brien, C.R. Brazier, and P.F. Bernath, J. Mol. Spectrosc. **130**, 33 (1988).
[21] C.R. Brazier and P.F. Bernath, J. Phys. Chem. **91**, 4548 (1989).
[22] C.N. Jarman and P.F. Bernath, J. Chem. Phys. **98**, 6697 (1993).
[23] C.N. Jarman and P.F. Bernath, J. Chem. Phys. **97**, 1711 (1992).
[24] W.T.M.L. Fernando, R.S. Ram. L.C. O'Brien, and P.F. Bernath, J. Phys. Chem. **95**, 2665 (1991).
[25] P.F. Bernath, Science **254**, 665 (1991).
[26] L.C. O'Brien, C.R. Brazier, S. Kinsey-Neilson, and P.F. Bernath, J. Phys. Chem. **94**, 3543 (1990).
[27] F.S. Pinalto, A.M.R.P. Bopegedera, W.T.M.L. Fernando, R. Hailey, L.C. O'Brien, C.R. Brazier, P.C. Keller, and P.F. Bernath, J. Am. Chem. Soc. **112**, 7900 (1990).
[28] C.R. Brazier, L.C. Ellingboe, S. Kinsey-Neilson, and P.F. Bernath, J. Am. Chem. Soc. **108**, 2126 (1986).
[29] A.M.R.P. Bopegedera, W.T.M.L. Fernando, and P.F. Bernath, J. Phys. Chem. **94**, 3547 (1990).
[30] W.T.M.L. Fernando, M. Douay, and P.F. Bernath, J. Mol. Spectrosc. **144**, 344 (1990).
[31] S.F. Rice, H. Martin, and R.W. Field, J. Chem. Phys. **82**, 5023 (1985).
[32] J. M. Mestdagh and J. Visticot, Chem. Phys. **155**, 79 (1991).
[33] J.V. Ortiz, J. Chem. Phys. **92**, 6728 (1990).
[34] T. Törring, W.E. Ernst, and S. Kindt, J. Chem. Phys. **81**, 4614 (1984).
[35] T.C. Steimle, D.A. Fletcher, K.Y. Jung, and C.T. Scurlock, J. Chem. Phys. **96**, 2556 (1992).

[36] R.F. Wormsbecher, R.E. Penn, and D.O. Harris, J. Mol. Spec. **97**, 65 (1983).
[37] C. Whitham and C. Jungen, J. Chem. Phys. **93**, 1001 (1990).
[38] A.J. Marr, M. Tanimoto, D. Goodridge, and T.C. Steimle, J. Chem. Phys. **103**, 4466 (1995).
[39] C. Zhao, P.F. Bernath, and J.W. Hepburn (unpublished).
[40] C. Zhao, P.G. Hajigeorgiou, P.F. Bernath, and J.W. Hepburn, J. Mol. Spectrosc. **176**, 268 (1996).
[41] S. Gerstenkorn and P. Luc, *Atlas du Spectre d'Asorption de la Molécule d'Iode* (CNRS II, 91405 Orsay, France, 1978).
[42] S. Gerstenkorn and P. Luc, Rev. Phys. Appl. **14**, 791 (1978).
[43] A.M.R.P Bopegedera, C.R. Brazier, and P.F. Bernath, J. Phys. Chem. **91**, 2779 (1987).
[44] F.W. Loomis and R.W. Wood, Phys. Rev. **32**, 223 (1928).
[45] J.K.G. Watson, J. Chem. Phys. **46**, 1935 (1967).
[46] J.M. Brown and T.J. Sears, J. Mol. Spectrosc. **75**, 111 (1979).
[47] J.K.G. Watson, in *Aspects of Quartic and Sextic Centrifugal Effects on Rotational Energy Levels*, Vol. 6 in *Vibrational Spectra and Structure*, edited by J.R. Durig (Elsevier, Amsterdam, 1977).
[48] E. Hirota, *High-Resolution Spectroscopy of Transient Molecules*, Vol. 40 in *Springer Series in Chemical Physics* (Springer, Berlin, 1985).
[49] See AIP document no. PAPS JCPSA-106-4860-3 for 3 pages of tables. Order by PAPS number and journal reference from American Institute of Physics, Physics Auxiliary Publication Service, Carolyn Gehlbach, 500 Sunnyside Boulevard, Woodbury, New York 11797–2999. Fax. (516) 576-2223, e-mail: paps@aip.org. The price is $1.50 for each microfiche (98 pages) or $5.00 for photocopies of up to 30 pages, and $0.15 for each additional page over 30 pages. Airmail additional. Make checks payable to the American Institute of Physics.
[50] J.H. Van Vleck, Rev. Mod. Phys. **23**, 213 (1965).
[51] G. Duxbury, *Molecular Spectroscopy*, Vol. 3 in *Specialist Periodical Reports* (The Chemical Society, Burlington House, London, 1975).
[52] R.F. Curl, Mol. Phys. **9**, 585 (1965).
[53] R.N. Dixon, Mol. Phys. **10**, 1 (1965).
[54] R.N. Dixon, Mol. Phys. **13**, 77 (1967).
[55] R.F. Curl, J. Chem. Phys. **37**, 779 (1962).
[56] L.M Tack, N.H. Rosenbaum, J.C. Owrutsky, and R.J. Saykally, J. Chem. Phys. **84**, 7056 (1986).
[57] K. Su, X. Hu X. Li, Y. Wang and Z. Wen, Chem. Phys. Lett. **258**, 431 (1996).
[58] I. Mills *et al.*, *Quantities, Units and Symbols in Physical Chemistry* (Blackwell Scientific, Oxford, 1988).
[59] W. Chan and I. Hamilton (unpublished).